Understanding degenerate ground states of a protected quantum circuit in the presence of disorder

Joshua M. Dempster,[1] Bo Fu,[1] David G. Ferguson,[1,*] D. I. Schuster,[2] and Jens Koch[1]
[1]*Department of Physics & Astronomy, Northwestern University, Evanston, Illinois 60208, USA*
[2]*Department of Physics and James Franck Institute, University of Chicago, Chicago, Illinois 60637, USA*
(Received 16 April 2014; revised manuscript received 16 July 2014; published 24 September 2014)

A recent theoretical proposal suggests that a simple circuit utilizing two superinductors may produce a qubit with ground-state degeneracy [Brooks, Phys. Rev. A **87**, 052306 (2013)]. We perform a full circuit analysis along with exact diagonalization of the circuit Hamiltonian to elucidate the nature of the spectrum and low-lying wave functions of this 0-π device. We show that the ground-state degeneracy is robust to disorder in charge, flux, and critical current as well as insensitive to modest variations in the circuit parameters. Our treatment is nonperturbative, provides access to excited states and matrix elements, and is immediately applicable also to intermediate parameter regimes of experimental interest.

DOI: 10.1103/PhysRevB.90.094518 PACS number(s): 03.67.Lx, 85.25.Hv, 85.25.Cp

I. INTRODUCTION

The idea of topological protection from decoherence [1] has greatly influenced research aimed at the physical implementation of quantum computation. The central paradigm of topological protection is to store quantum information in an explicitly nonlocal fashion, rendering qubits insensitive to various sources of local noise. Potential realizations of such topological protection have been suggested for anyon quasiparticles in fractional quantum Hall systems [1–3], for $p+ip$ superconductors [4], as well as for Majorana fermions in topological nanowires [5–10]. With coherence times of the order of milliseconds [11,12], conventional unprotected superconducting circuits [13–16] are already quite promising [17,18]. Here we will attempt to explore what are the minimal requirements for such intrinsic protection in superconducting circuits. We will show that the use of circuits with more than one or two effective degrees of freedom can lead to qualitatively different and more robust quantum states.

A promising avenue for realizing protection in superconducting circuits is to exploit frustration, such as topological or Ising-type frustration in junction arrays first proposed in [19,20] and further explored in [21–23]. From this viewpoint, the recently proposed 0-π circuit by Brooks, Kitaev and Preskill (BKP) [24] is particularly intriguing: it features a much smaller four-node superconducting circuit with the potential of remarkable robustness with respect to local noise and the possibility of carrying out quantum gates in a protected fashion.

The BKP paper takes it for granted that a 0-π qubit with sufficient inductance and without disorder can be realized, and rather focuses on protected gates to be performed on this device. A challenge of the circuit is, indeed, that its predicted properties may require inductances larger than those that have been realized to date. Nevertheless, there have been significant experimental advances towards building such "superinductors" with increasingly large inductances [25–28].

Our paper has two primary goals. First, we wish to elucidate the central physics underlying the 0-π circuit by studying the nature of its wave functions and general spectral properties. Second, we investigate what device parameters are needed for robust degeneracy and discuss the feasibility of accessing this parameter regime based on state-of-the-art fabrication techniques. This discussion necessarily includes the effects of device imperfections, in particular disorder in circuit element parameters, on the characteristics of the 0-π circuit.

The presentation is structured as follows. We start with the full circuit analysis of the 0-π device in Sec. II, and thereby identify its three relevant degrees of freedom. If disorder in device parameters is absent, the 0-π device is described by merely two degrees of freedom, while the third one decouples. For this ideal case, we investigate the spectrum, wave functions, and the degeneracy of low-lying states in Sec. III. The role of disorder in circuit parameters is addressed in Sec. IV. We show that the 0-π circuit is favorably insensitive to disorder in junction parameters but may be negatively affected by disorder in the values of the superinductances and the additional capacitances in the circuit. We present our conclusions and an outlook on possible future uses of the 0-π circuit in Sec. V.

II. CIRCUIT ANALYSIS OF THE SYMMETRIC 0-π DEVICE

The 0-π device, depicted in Fig. 1, is a superconducting circuit with four nodes. The nodes form an alternating ring consisting of two inductors and two Josephson junctions. Additional cross capacitances connect the opposing nodes in the ring. As shown, all circuit elements occur pairwise and are, in the ideal circuit, identical such that both Josephson junctions share the same Josephson energy E_J and junction capacitance C_J, both inductances are given by L, and both cross capacitances by C. Neglecting any deviations in these circuit element parameters renders the circuit symmetric under a π rotation. (For better visibility, one cross capacitance is shown external to the ring in Fig. 1.) We hence refer to this special case as the *symmetric* 0-π device.

For the quantitative study of the spectrum and eigenstates of the symmetric 0-π device, we begin with a systematic circuit analysis. In the usual first step [29,30], we assign node fluxes to each of the four circuit nodes numbered $j=1,\ldots,4$. Each node flux, defined as the time integral of the

[*]Present address: Advanced Concepts and Technologies Division, Northrop Grumman Corporation, Linthicum, Maryland 21090, USA.

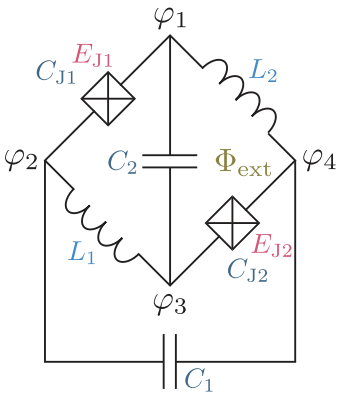

FIG. 1. (Color online) Circuit diagram of the 0-π qubit. Each of the four circuit nodes is associated with one phase variable φ_j. Additional symbols show the naming of capacitances, inductances, and Josephson-junction parameters, and the magnetic flux Φ_{ext} that may thread the inner circuit loop.

electrostatic potential U_j on each node, serves as a generalized variable in the circuit Lagrangian. For convenience, we employ the dimensionless version of the node variables, $\varphi_j = \int_{t_0}^{t} dt' U_j(t')/\Phi_0$, where $\Phi_0 = \hbar/2e$ is the reduced magnetic-flux quantum. (Note the inclusion of the $1/2\pi$ factor relative to the conventional definition of the magnetic-flux quantum).

Expressed in terms of node variables, the kinetic- and potential-energy contributions to the circuit Lagrangian assume the form

$$T = \tfrac{1}{2}\mathsf{C}_\mathrm{J}(\dot\varphi_2 - \dot\varphi_1)^2 + \tfrac{1}{2}\mathsf{C}_\mathrm{J}(\dot\varphi_4 - \dot\varphi_3)^2 + \tfrac{1}{2}\mathsf{C}(\dot\varphi_3 - \dot\varphi_1)^2 + \tfrac{1}{2}\mathsf{C}(\dot\varphi_4 - \dot\varphi_2)^2 \quad (1)$$

and

$$U = -E_\mathrm{J}\cos(\varphi_4 - \varphi_3 - \varphi_{ext}/2) - E_\mathrm{J}\cos(\varphi_2 - \varphi_1 - \varphi_{ext}/2) + \tfrac{1}{2}E_L(\varphi_2 - \varphi_3)^2 + \tfrac{1}{2}E_L(\varphi_4 - \varphi_1)^2. \quad (2)$$

Note that we have absorbed factors of Φ_0^2 by letting $\mathsf{C} = C\Phi_0^2$, etc. The potential energy U incorporates the effect of an external magnetic flux, expressed here in dimensionless form as $\varphi_{ext} = \Phi_{ext}/\Phi_0$. We have chosen a symmetric division of the flux between the two Josephson junctions. (As usual, other equivalent choices are simply obtained by shifting the node variables.) The terms in the second line of Eq. (2) denote the inductive contributions in terms of the energy $E_L = \Phi_0^2/L$.

From Eq. (1) it is clear that there will be cross terms between the $\dot\varphi_j$ variables. Physically, such terms arise because of cross capacitances in the circuit diagram, Fig. 1. We now adopt new variables ϕ, θ, χ, and Σ, which we will show to diagonalize the kinetic-energy term and which are defined as

$$2\phi = (\varphi_2 - \varphi_3) + (\varphi_4 - \varphi_1), \quad 2\chi = (\varphi_2 - \varphi_3) - (\varphi_4 - \varphi_1),$$
$$2\theta = (\varphi_2 - \varphi_1) - (\varphi_4 - \varphi_3), \quad \Sigma = \varphi_1 + \varphi_2 + \varphi_3 + \varphi_4 \quad (3)$$

with inverse

$$2\varphi_1 = \Sigma - \theta - \phi + \chi, \quad 2\varphi_2 = \Sigma + \theta + \phi + \chi,$$
$$2\varphi_3 = \Sigma + \theta - \phi - \chi, \quad 2\varphi_4 = \Sigma - \theta + \phi - \chi. \quad (4)$$

Following our variable transformation, the kinetic and potential energies simplify to

$$T = \mathsf{C}_\mathrm{J}\dot\phi^2 + \mathsf{C}_\Sigma\dot\theta^2 + \mathsf{C}\dot\chi^2 \quad (5)$$

and

$$U = -2E_\mathrm{J}\cos\theta\cos(\phi - \varphi_{ext}/2) + E_L\phi^2 + E_L\chi^2. \quad (6)$$

Here, $\mathsf{C}_\Sigma = \mathsf{C}_\mathrm{J} + \mathsf{C}$ abbreviates the sum capacitance, again including the factor of Φ_0^2. As intended, the effective mass tensor in Eq. (5) is now diagonal. Due to gauge invariance, the variable Σ decouples completely, leaving us with three degrees of freedom. Furthermore, the variable χ is harmonic: it simply captures the oscillator subsystem with frequency $\Omega_\chi = \sqrt{8E_L E_\mathrm{C}}/\hbar$ formed by the two inductances L and the two capacitances C; $E_\mathrm{C} = e^2/2C$ denotes the relevant charging energy. For the perfectly symmetric circuit, the oscillator variable χ exactly decouples from the other two variables θ and ϕ but will become relevant again once we consider disorder in Sec. IV.

For the remaining two degrees of freedom of the symmetric 0-π qubit we thus obtain the effective Lagrangian

$$\mathcal{L}_{sym} = \mathsf{C}_\mathrm{J}\dot\phi^2 + \mathsf{C}_\Sigma\dot\theta^2 + 2E_\mathrm{J}\cos\theta\cos(\phi - \varphi_{ext}/2) - E_L\phi^2. \quad (7)$$

Note that, here, $\dot\phi$ only sees the junction capacitance, whereas $\dot\theta$ sees (i.e., depends on the phase difference across) both the junction as well as the other two cross capacitances. The new effective masses associated with them may thus be different and will be instrumental in understanding the physics of the circuit. From the potential-energy terms it is clear that both ϕ and θ are affected by the junctions, but only ϕ is influenced by the inductors.

Carrying out the usual Legendre transform and canonical quantization, we finally arrive at

$$H_{sym} = -2E_{C\mathrm{J}}\partial_\phi^2 - 2E_{C\Sigma}\partial_\theta^2 - 2E_\mathrm{J}\cos\theta\cos(\phi - \varphi_{ext}/2) + E_L\phi^2 + 2E_\mathrm{J} \quad (8)$$

as the Hamiltonian of the symmetric 0-π qubit. The additional energy shift $2E_\mathrm{J}$ included in H is convenient in rendering the energy spectrum strictly positive. All charging energies in H refer to the charge of a single electron so that $E_{C\mathrm{J}} = e^2/2C_\mathrm{J}$ and $E_{C\Sigma} = e^2/2C_\Sigma$. The potential energy $V(\phi,\theta)$ associated with the symmetric $0-\pi$ Hamiltonian is depicted in Fig. 2(a). The boundary conditions associated with H_{sym} consist of square-integrability of the wave functions $\Psi(\phi,\theta)$ along the real ϕ axis and 2π periodicity in the θ variable.

III. SPECTRUM OF THE SYMMETRIC 0-π DEVICE

A. Qualitative discussion

The effective potential for the 0-π circuit derived in Eq. (8), $V(\phi,\theta) = -2E_\mathrm{J}\cos\theta\cos(\phi - \varphi_{ext}/2) + E_L\phi^2 + 2E_\mathrm{J}$, is shown in Fig. 2(a). For a qualitative understanding of low-lying eigenstates of the 0-π device, it is useful to consider

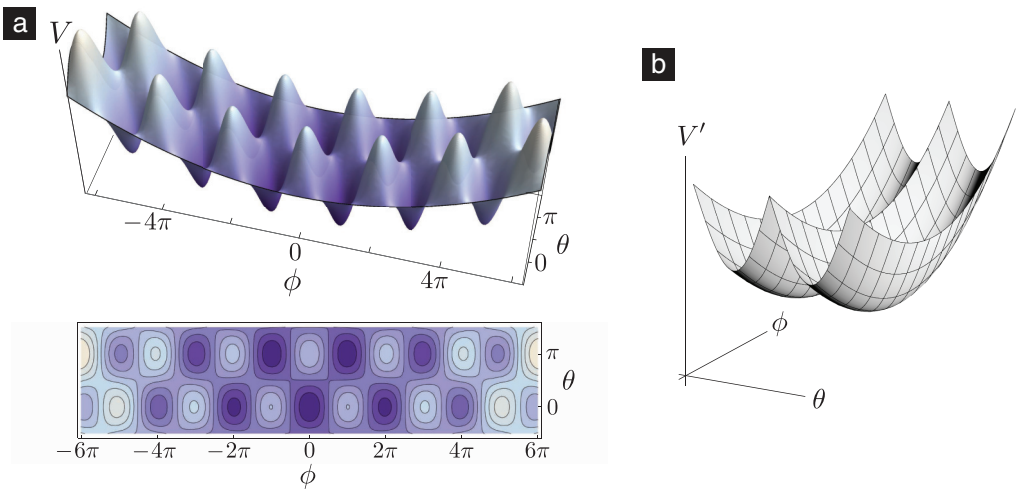

FIG. 2. (Color online) (a) Potential energy $V(\phi,\theta)$, showing the twofold fluxoniumlike potential for cuts along the $\theta = 0$ and $\theta = \pi$ ridges. Localization wave function in these ridges occurs when the effective mass along the θ direction is sufficiently large. (Parameters: $E_J/E_L = 165$.) (b) Simplified model with separable potential energy. In this case, wave functions are products $\psi(\phi,\theta) = \psi_{ho}(\phi)\,\psi_{dw}(\theta)$ of harmonic-oscillator and double-well wave functions along ϕ and θ direction, respectively.

a much simpler potential first, taking the form

$$V'(\phi,\theta) = V_{dw}(\theta) + V_{ho}(\phi). \tag{9}$$

Here, V_{dw} is a symmetric double-well potential and V_{ho} a shallow harmonic oscillator potential as shown in Fig. 2(b). Due to the special form of this potential, the problem becomes separable and wave functions are products $\psi(\phi,\theta) = \psi_{ho}(\phi)\,\psi_{dw}(\theta)$ of harmonic-oscillator and double-well wave functions along the ϕ and θ coordinate, respectively. The two lowest-lying eigenstates correspond to Gaussian wave functions along ϕ and the symmetric and antisymmetric superposition of states localized close to the the two double-well minima along the θ direction. The degeneracy of these two states is only weakly broken by tunneling as long as the effective mass along the θ direction is heavy enough to suppress large fluctuations. For a charge space discussion of the structure and degeneracy of this separable model see Appendix B 1.

As long as tunneling in the θ direction remains suppressed, excited states above these lowest two states will appear in doublets. Except for the small tunnel-induced splittings within doublets, level spacings in the spectrum will exhibit two separate energy scales: the harmonic-oscillator energy spacing from V_{ho} and the spacing of states in each local-well of V_{dw}. When considering the form of the wave functions, the two energy spacings are associated with either an increase in the node number in the ϕ direction or in the θ direction. An example for the choice $V_{dw}(\theta) = -2E_J|\cos\theta|$ is shown in Fig. 3(b), illustrating the localization along the two ridges $\theta = 0$ and $\theta = \pi$ as well as the progressive increase in the number of nodes along the two directions.

We next consider the actual potential energy V of the symmetric 0-π circuit, as shown in Fig. 2(a) for zero magnetic flux. Like the simplified potential V', the true potential V has two ridges at $\theta = 0$ and $\theta = \pi$—but additionally has oscillatory terms along the ϕ direction. While each of them resembles a fluxonium potential [25,31], the minima in the $\theta = 0$ ridge versus the $\theta = \pi$ ridge are staggered with respect to one another (thus preventing separability). With the appropriate choice of circuit parameters, the interesting ground-state degeneracy seen in the simplified toy model is also reflected in the physics of the actual circuit with the more complicated potential.

B. Discussion of conditions for degeneracy

A prototype for a single-particle nearly degenerate system is a double well. In the mentioned toy model, it is clear that if the valleys are symmetric and tunneling is suppressed, then the states of the particle living in the left and right valley will be approximately decoupled and degenerate. For certain circuit parameters, the degeneracy in the 0-π circuit is very similar in nature. It will become apparent in Sec. IV that the degeneracy of the 0-π circuit is especially robust against disorder.

When tunneling in the ϕ direction (i.e., in the direction along each ridge) is much larger than tunneling in the θ direction (from one ridge to the other), then the maxima in the 0-π potential can largely be ignored and one expects a similar degeneracy as in the toy model. This difference in tunneling strengths can be achieved by choosing significantly different effective masses along the ϕ and θ directions, namely $E_{CJ} \gg E_{C\Sigma}$ (or, equivalently, $C_J \ll C$). Localization along θ within each ridge is further strengthened by reducing the oscillator length for harmonic fluctuations along the θ direction, which is accomplished when $E_J \gg E_{C\Sigma}$.

The symmetry between the two ridges is broken because the minima of the two ridges are staggered with respect to the harmonic potential. Further, magnetic flux shifts both ridges with respect to the harmonic potential, leading to energy offsets. The sensitivity to both of these effects is reduced when wave functions are delocalized over multiple minima of the cosine potential within each ridge. This occurs when the parabolic envelope of the potential is sufficiently shallow, i.e., $E_L \ll E_J$, and the nominal oscillator length in the quadratic potential is large, i.e., $E_L \ll E_{CJ}$.

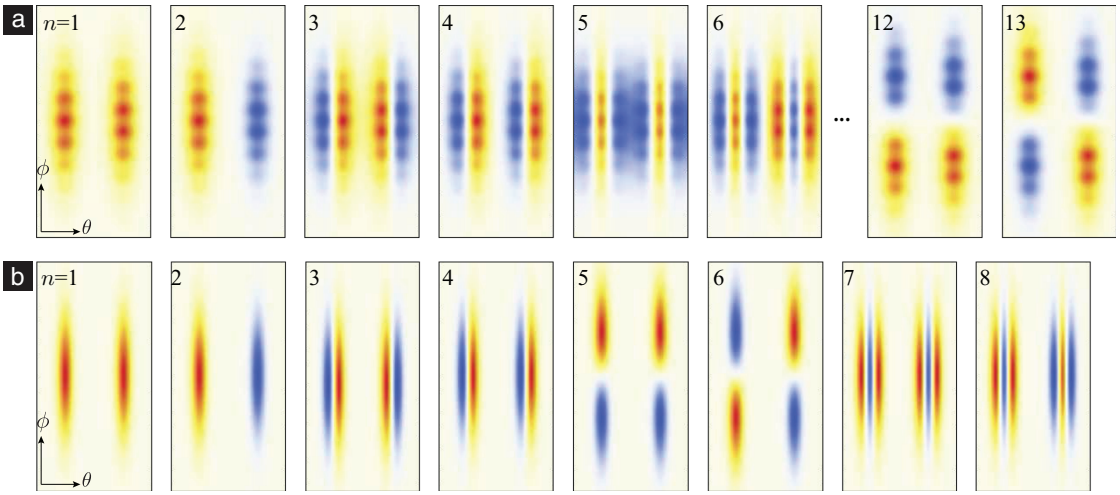

FIG. 3. (Color online) Density plots of the wave function amplitudes for eigenstates in (a), the full potential V of the 0-π qubit and (b), the separable potential V'. The numbers $n = 1,2,\ldots$ enumerate the eigenstates starting from the ground state. Different colors (shades of gray) mark distinct signs of the wave function amplitudes. In the simpler case (b), localization along the two ridges $\theta = 0$ and $\theta = \pi$ and pairing of states into doublets of symmetric and antisymmetric states (in θ direction) are easily visible. Wave functions of the actual 0-π circuit in (a) show additional local extrema due to the cosine corrugation of the potential V. Overall comparison—in particular, states $n = 5$ and 6—shows that delocalization in θ occurs more easily for the 0-π circuit. As a result, the development of nodes in ϕ direction (states 12 and 13) only takes place at higher energies. (Parameter values: $\hbar\omega_p/E_L = 10^4$, $\hbar\omega_p/E_{C\Sigma} = 2.2\times10^3$, $\hbar\omega_p/E_J = 7.9$.)

Intuition for this insensitivity of states delocalized in ϕ is similar to the flux insensitivity of the fluxonium circuit [31,32]. There, low-lying wave functions form metaplasmon states delocalized across multiple potential minima. These states are exponentially insensitive, with an exponential suppression factor of $\sim\exp(-r\sqrt{\epsilon/E_L})$ where ϵ is the charge dispersion of the Cooper pair box with energy scales E_J and E_{CJ}, and the constant $r > 0$ is of order unity [31,33]. We will show that the same physics leads to degenerate states insensitive to magnetic flux and energy offsets in the 0-π circuit.

To summarize, we find that robust ground-state degeneracy (up to exponentially small deviations) requires the following set of inequalities among device parameters to hold:

$$E_L, E_{C\Sigma} \ll E_J, E_{CJ}. \tag{10}$$

An analysis of the ground-state degeneracy in this limit, from the perspective of the charge basis, is given in Appendix B.

C. Numerical results for wave functions and energy levels

Due to the cosine modulation along the ϕ direction and coupling between motion in the ϕ and θ direction, the full potential V of the 0-π circuit is not separable. We thus solve the corresponding Schrödinger equation numerically to obtain energy levels and eigenstates. Specifically, we employ the finite-difference method in its simplest implementation (see Appendix A). With this method we can find the full solution in both the limit described in Eq. (10) but also in intermediate regimes where no clear hierarchy of energy scales exists.

Figure 3(a) illustrates the resulting wave functions for the 0-π device deep in the degeneracy regime. Qualitative similarities with the wave functions of the simplified potential [Fig. 3(b)] are evident. Important differences between the two cases include the additional structure of wave functions of the 0-π device brought on by the cosine corrugation of the potential, as well as an increased tendency of wave functions to spread in the θ direction. The latter is easily understood from inspection of the potential V, showing that the two ridges are not separated by a large potential barrier along $\theta = \pi/2$. Nevertheless, the wave functions shown in Fig. 3 are qualitatively similar between the toy model and the actual potential.

Which of these two types is formed generally depends on the parameters E_L, $E_{C\Sigma}$, and magnetic flux. As long as the magnetic flux is away from half-integer flux quanta, the staggering of local minima leads to an effective energy offset between the two ridges. Just as for an asymmetric double-well potential these energy offsets promote localization in the individual ridges, becoming more pronounced as E_L is increased and leading to a ground-state doublet of the type shown in Fig. 4(a) [Fig. 9(a) shows the charge basis representation of the doublet]. Conversely, decreasing the effective mass along the θ direction, i.e., increasing $E_{C\Sigma}$, promotes tunneling and delocalization of the wave function, leading to eigenstates in the form of symmetric and antisymmetric superpositions, as shown in Fig. 4(b) [Fig. 9(b) shows the charge basis representation of the doublet]. In summary, by tuning the relative strength between E_L and the tunneling (via $E_{C\Sigma}$), we can favor one type over the other.

In principle, magnetic flux can also be used to generate superposition-type states: tuning Φ_{ext} to a half-integer flux quantum produces a potential which is symmetric with respect to the two ridges and, thus, does not exhibit an effective energy offset. Figure 5 gives an example of the full flux dependence of low-lying energy levels. The doublet structure of the lowest four energy states is clearly visible, as is the suppression of the energy splitting at half-integer flux ($\varphi_{ext} = \pi$). The metaplasmonlike character of the wave functions explains the relative insensitivity of low-lying energy levels to the external magnetic flux.

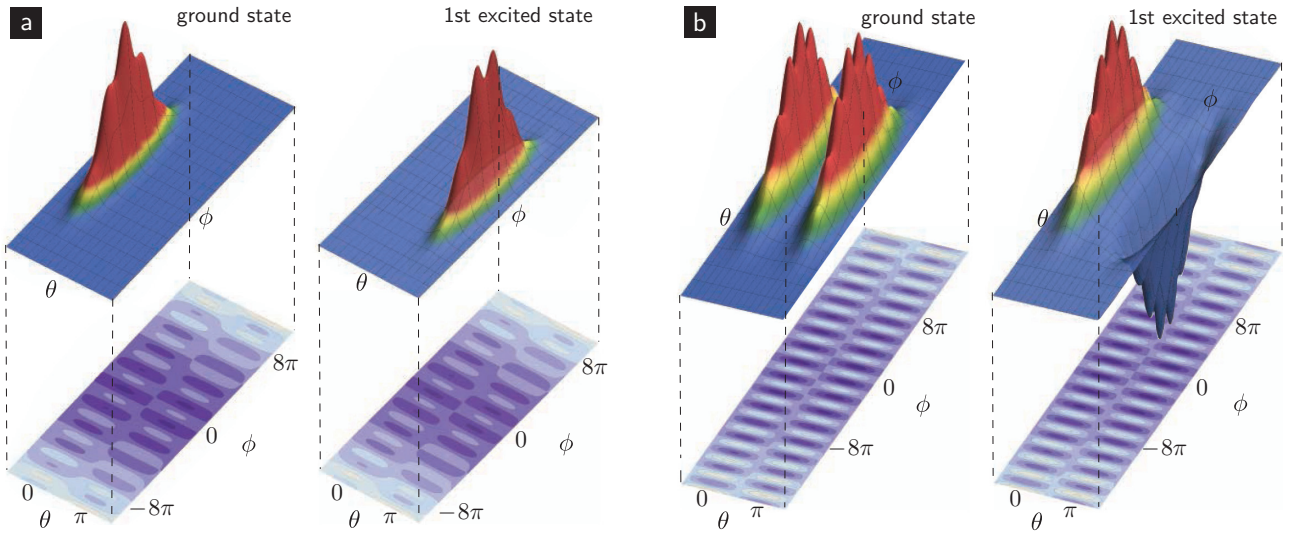

FIG. 4. (Color online) Wave functions for the ground state and its (nearly) degenerate partner state for two choices of device parameters. While the value of the degeneracy is identical in the two cases ($D = 2.7$), it is limited by potential-energy differences in the two ridges in (a), and by tunneling along the θ direction in (b). For tunneling-induced degeneracy breaking (larger $E_{C\Sigma}$ and smaller E_L), we observe symmetric and antisymmetric superpositions of the states localized in the individual ridges. For degeneracy breaking due to potential offsets between the two ridges (smaller $E_{C\Sigma}$ and larger E_L), we observe localization in the two separate ridges. Figure 9 displays the same eigenfunctions expressed in the charge basis. [Parameter values: (a) $\hbar\omega_p/E_L = 9.9\times10^2$, $\hbar\omega_p/E_{C\Sigma} = 10^4$, $\hbar\omega_p/E_J = 8.3$; (b) same as in Fig. 3, i.e., $\hbar\omega_p/E_L = 10^4$, $\hbar\omega_p/E_{C\Sigma} = 2.2\times10^3$, $\hbar\omega_p/E_J = 7.9$.]

We next assess the degree of degeneracy that can be achieved with realistic device parameters. To quantify the degeneracy we define the parameter D by

$$D = \log_{10}\frac{E_2 - E_0}{E_1 - E_0}, \tag{11}$$

where E_0, E_1, and E_2 are the eigenenergies arranged in increasing order, starting with the ground state. D thus specifies the ratio between the doublet energy splitting and the energy difference to the next higher doublet on a log scale, as illustrated in Fig. 5. In the absence of magnetic flux, wave functions in this example are of the type shown in Fig. 4(a). The degeneracy D is seen to reach a maximum at half-integer flux, which eliminates the energy offsets between the two ridges and switches to wave functions of the Fig. 4(b) type. The following discussion will investigate the degeneracy at zero flux, away from the special flux value, to better highlight the interplay between the two regimes.

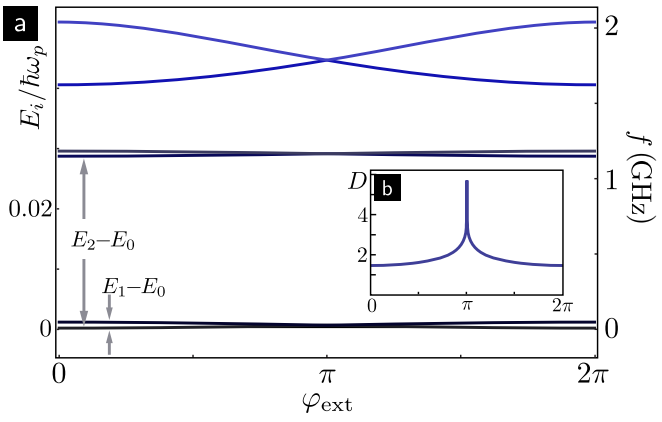

FIG. 5. (Color online) (a) Energy spectrum as a function of external magnetic flux $\varphi_{ext} = \Phi_{ext}/\Phi_0$. For the selected parameters, the lifting of the degeneracy at zero flux is primarily induced by the potential asymmetry and strongly suppressed for $\varphi_{ext} = \pi$ where the potential becomes symmetric. (b) Magnetic-flux dependence of the logarithmic degeneracy parameter D. (Parameter values: $\hbar\omega_p/E_L = 10^3$, $\hbar\omega_p/E_{C\Sigma} = 10^3$, and $\hbar\omega_p/E_J = 3.95$.)

An important question is the quantitative dependence of the degeneracy D on the device parameters of the 0-π circuit. Indeed, the inequalities from Eq. (10) specify general requirements for finding near-degenerate pairs of low-lying states, however, Eq. (10) does not provide a concrete parameter range. To obtain this range, we systematically calculate the degeneracy D for a large set of parameter choices as follows. We first note that variations in junction capacitance C_J and Josephson energy E_J are routinely achieved with Al-AlOx-Al junctions by changing the junction area while keeping the insulator thickness constant. Under these circumstances, the effective plasma frequency $\omega_p = \sqrt{8E_JE_{CJ}}/\hbar$ remains fixed. We thus take $\hbar\omega_p$ as our energy scale and treat E_L, $E_{C\Sigma}$, and E_J as independent parameters; the junction capacitance takes the form $E_{CJ}/\hbar\omega_p = \hbar\omega_p/8E_J$. We then form a logarithmic grid in the parameter plane spanned by E_L and $E_{C\Sigma}$. For each grid point, we calculate the degeneracy D and finally vary E_J to find the maximum degeneracy value D_{max} (for given E_L and $E_{C\Sigma}$). Our key results are depicted in the log-log plot shown in Fig. 6.

The constant-D contours in Fig. 6 illustrate that there are indeed two qualitative regimes for reaching high degeneracy values, which is fully consistent with the two types of doublet states shown in Fig. 4. Whenever E_L is sufficiently small, the degeneracy D is mainly limited by the splitting induced by tunneling along the θ direction. Accordingly, D can be

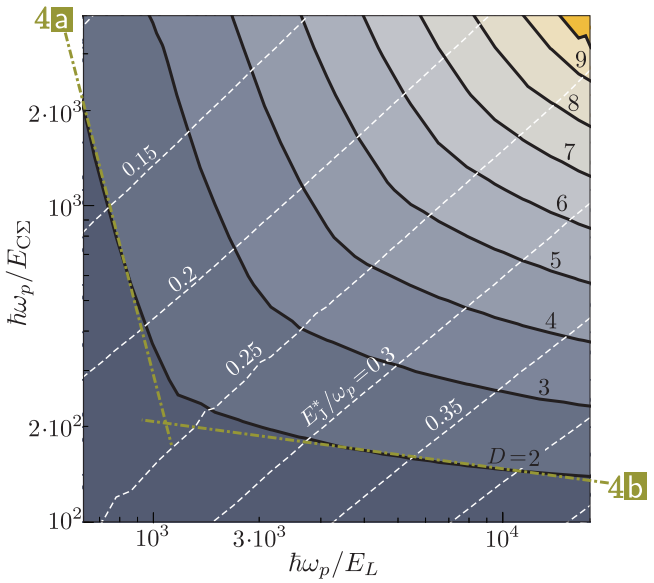

FIG. 6. (Color online) Maximum value of the degeneracy parameter D for given E_L and $E_{C\Sigma}$ and optimal E_J^*. Contours of maximum D are shown in black and show that strong degeneracy requires challengingly small values of E_L and $E_{C\Sigma}$. Contours for the optimal values E_J^* maximizing D are shown as white dashed lines. The two dash-dotted asymptotes show the regime where D is limited by potential offsets [towards larger E_L, where wave functions have the form of Fig. 4(a)] and the regime where D is limited by tunnel splitting [towards smaller E_L, where wave functions have the form of Fig. 4(b)].

increased by further suppressing tunneling, as is achieved by decreasing the value of $E_{C\Sigma}$. In this regime, wave functions are symmetric and antisymmetric superpositions of wave functions localized in the $\theta = 0$ and $\theta = \pi$ ridges, as shown in Fig. 4(b). Vice versa, when $E_{C\Sigma}$ is sufficiently small, D is predominantly governed by the asymmetry between the two potential ridges. This asymmetry can be lowered by decreasing the superinductance energy E_L. Wave functions in this regime are localized in one ridge or the other; see Fig. 4(a).

In Fig. 6, we also show the contours for E_J^*, defined as the value of E_J that maximizes the degeneracy for given E_L and $E_{C\Sigma}$. These contours are, approximately, straight and parallel lines with a unit slope, implying that the optimum values obey the parametric dependence $E_J^* = f(E_{C\Sigma}/E_L)$. Contours of E_J^* are nearly equidistant, implying that E_J^* is nearly a plane surface in log-log space over the investigated parameter range. Numerically, we find the approximate relation

$$\frac{E_J^*}{\hbar\omega_p} \approx 0.17 - 0.11 \times \log_{10}(E_{C\Sigma}/E_L). \tag{12}$$

To illustrate the practical challenge in reaching the parameter regime of degeneracy, let us consider a specific example of parameter values. We choose $\hbar\omega_p/E_{C\Sigma} = \hbar\omega_p/E_L = 10^3$ for the relevant charging and superinductance energies, which achieves a degeneracy value of $D \approx 2$; see Fig. 6. For Josephson junctions with a plasma oscillation frequency of the order of $\omega_p/2\pi = 40$ GHz (typical of Al-AlOx junctions), this choice implies a superinductance of roughly 4 μH and a capacitance C of about 0.5 pF.

Experimentally, capacitances of the order of 0.1 pF (charging energies in the range of 200 MHz) are routinely achieved in transmon qubits [11] and could be increased further to the desired level. The largest values of superinductances, to date, are $L = 0.3$ μH in the linear regime [28] and $L = 3$ μH in the nonlinear regime [27]. Reaching a linear superinductance with the value of 4 μH from our example parameter set therefore remains challenging but may be possible assuming further advances in the design and fabrication of superinductances based on Josephson-junction arrays or thin superconducting wires.

Since the two lowest levels become nearly degenerate, it is appropriate to ask how temperature affects the circuit. Wave functions of the ground-state doublet are disjoint and will be coupled to each other only very weakly. Hence, it is possible to operate the circuit even when $k_B T \gg E_{01}$—quite similar to the use of hyperfine levels of trapped ions even at room temperature. In order to initialize and measure the state of the circuit, the energy separation to the next set of levels should exceed the energy scale set by temperature, $E_{02} \gg k_B T$—in analogy to the optical transitions used in ions. For the parameters considered here, E_{02} is of the order of 1 GHz (Fig. 5), corresponding to a temperature of 50 mK which is readily achievable with standard dilution refrigerators.

We note that the value $D = 1$ of the degeneracy parameter may be viewed as a threshold above which protection becomes manifest. Specifically, appropriate changes in circuit parameters beyond this point lead to an *exponential* gain in protection from decoherence. Given the discussion of the example parameter set, we find that reaching the $D = 1$ threshold is completely feasible with current technology and the interesting physics of the circuit should be readily observable. However, to supplant existing superconducting qubits—which already are remarkably good—higher values of D will be necessary, requiring advances in fabrication as well as further development of protocols for single- and multiqubit operations.

IV. EFFECTS OF DISORDER

Unavoidable device imperfections will generally lead to some amount of disorder in the parameters of the 0-π circuit. Specifically, the parameters of each pair of junctions, capacitors, and superinductors in the circuit will not be precisely identical. We thus consider the effect of such disorder on the spectrum of the 0-π circuit and on the degeneracy D, in particular.

When including parameter disorder, the kinetic and potential energies [previously Eqs. (5) and (6)] take the more general form

$$T = \mathsf{C}_\mathrm{J}\dot{\phi}^2 + (\mathsf{C} + \mathsf{C}_\mathrm{J})\dot{\theta}^2 + \mathsf{C}\dot{\chi}^2 + 2\,\delta\mathsf{C}_\mathrm{J}\,\dot{\phi}\,\dot{\theta} + 2\delta\mathsf{C}\,\dot{\theta}\,\dot{\chi} \tag{13}$$

and

$$\begin{aligned} U = &-2E_\mathrm{J}\cos(\theta)\cos\left(\phi - \tfrac{1}{2}\varphi_\mathrm{ext}\right) \\ &+ 2\delta E_\mathrm{J}\sin(\theta)\sin\left(\phi - \tfrac{1}{2}\varphi_\mathrm{ext}\right) \\ &+ E_L\phi^2 + E_L\chi^2 + 2\delta E_L\phi\chi\,. \end{aligned} \tag{14}$$

Here, $C = (C_1 + C_2)/2$ now denotes the arithmetic mean of the two capacitors and $\delta C = (C_1 - C_2)/2$ the deviation from the mean. We employ analogous definitions for disorder in the various other circuit parameters.

A Legendre transform and subsequent series expansion in the capacitive disorder then leads to the Hamiltonian

$$\begin{aligned} H \simeq\, & H_{\rm sym} + 4E_{\rm C\Sigma}(\delta C_{\rm J}/C_{\rm J})\partial_\phi\partial_\theta \\ & + 2\,\delta E_{\rm J}\sin\theta\,\sin(\phi - \varphi_{\rm ext}/2) - 2E_{\rm C}\partial_\chi^2 + E_L\chi^2 \\ & + 4E_{\rm C\Sigma}(\delta C/C)\partial_\theta\partial_\chi + 2\,\delta E_L\phi\,\chi, \end{aligned} \tag{15}$$

where we have dropped contributions $\sim\mathcal{O}(\delta C^2, \delta {C_{\rm J}}^2, \delta C\,\delta C_{\rm J})$. The terms in the first line of Eq. (15) comprise the previous model of the symmetric 0-π device [Eq. (8)] plus small corrections due to disorder in the parameters $C_{\rm J}$ and $E_{\rm J}$ describing the two Josephson junctions. The second line contains the harmonic terms for the χ degree of freedom, as well as two terms from disorder in E_L and C which couple between the χ degree of freedom and the fundamental 0-π circuit variables (ϕ, θ). In the following, we discuss the effects of these different types of disorder.

A. Disorder in junction parameters $E_{\rm J}$ and $C_{\rm J}$

Disorder in the Josephson junction parameters ($\delta E_{\rm J}$ and $\delta C_{\rm J}$) is straightforward to incorporate as it does not introduce coupling between the fundamental 0-π circuit variables and the additional harmonic degree of freedom captured by the χ variable. The effects of junction disorder can thus be treated by the same numerical diagonalization scheme as before.

As seen from Eq. (15), disorder in the junction capacitance $C_{\rm J}$ only leads to a slight change in the effective mass tensor. Corrections due to this are expected to be small since $E_{\rm C\Sigma}\,\delta C_{\rm J}/C_{\rm J} < E_{\rm C\Sigma} \ll E_{\rm CJ}$. The critical condition for maintaining robust degeneracy in the presence of $C_{\rm J}$ disorder, is that the tunneling along ϕ must remain strong and tunneling along θ must remain weak. As long as the $\delta C_{\rm J}$ (and $C_{\rm J}$) remains small compared to C, this tunneling condition will still be satisfied. Indeed, results from numerics show that the effect of this disorder is negligible for values up to $\delta C_{\rm J}/C_{\rm J} = 100\%$. This should be compared to the conservative estimate of experimental disorder in $C_{\rm J}$ of up to 10%, mainly caused by edge imperfections in the double-angle evaporation used for the fabrication of Al-AlOx Josephson junction.

Disorder in the Josephson energies leads to a distortion of the potential energy $V(\phi,\theta)$. According to Eq. (15), this distortion is directly proportional to $\delta E_{\rm J}$ and can hence produce noticeable changes in wave functions, eigenenergies, and the degeneracy measure D. Representative numerical results are shown in Fig. 7. The degeneracy D is fairly robust for realistic amounts of $E_{\rm J}$ disorder [Fig. 7(a)]. Experimentally, Josephson energies are known to vary from device to device by up to 20%; disorder among junctions within the same device is expected to be significantly smaller than this. The reason for the rapid drop of D at very strong disorder is illustrated in Fig. 7(b), showing the dramatic change of wave functions as the potential energy is more and more deformed. Strong $E_{\rm J}$ disorder eliminates the two potential ridges along $\theta = 0$ and $\theta = \pi$ and wave functions spread over the full range along the θ direction. Consequently, $E_{\rm J}$ disorder ultimately destroys the degeneracies of low-lying states—however, only for disorder strengths that vastly exceed the amount of disorder expected in experiments.

B. Disorder in C and E_L

Both disorder in the capacitance C as well as in the superinductance energy E_L introduce coupling between the 0-π device variables (ϕ,θ) and the harmonic variable χ. This is similar to the typical situation of circuit QED where a qubit is coupled to a harmonic oscillator, and can thus be treated by the same methods [34]. In the eigenbasis $\{|l\rangle\}_{l=0,1,\ldots}$ of the symmetric 0-π circuit [Eq. (8)], the full Hamiltonian can be rewritten as

$$H = \sum_l E_l^{\rm sym}|l\rangle\langle l| + \hbar\Omega_\chi a^\dagger a + \sum_{l,l'}(g_{ll'}|l\rangle\langle l'|a + {\rm H.c.}), \tag{16}$$

where $g_{ll'} = g^\phi_{ll'} + i g^\theta_{ll'}$ are coupling strengths defined by

$$g^\theta_{ll'} = E_{\rm C\Sigma}(\delta C/C)\,(32E_L/E_{\rm C})^{1/4}\,\langle\, l\,|\,i\,\partial_\theta\,|\,l'\,\rangle, \tag{17}$$

$$g^\phi_{ll'} = \delta E_L\,(8E_{\rm C}/E_L)^{1/4}\langle\, l\,|\,\phi\,|\,l'\,\rangle, \tag{18}$$

a ($a^\dagger$) is the annihilation (creation) operator for excitations of the χ oscillator, and $\Omega_\chi/2\pi$ is its angular frequency. (For

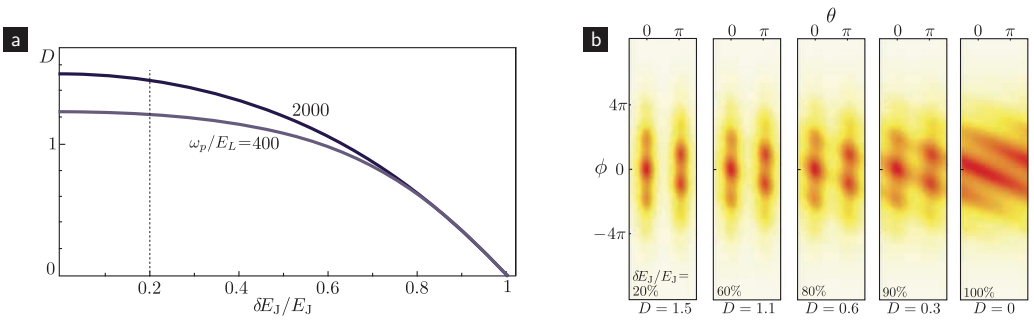

FIG. 7. (Color online) Effect of disorder in the Josephson energies. (a) Dependence of the degeneracy parameter D on relative disorder in the Josephson energy, $\delta E_{\rm J}/E_{\rm J}$. The plot shows a comparison of two different parameter sets, both with $\hbar\omega_p/E_{\rm C\Sigma} = 10^3$ and $\hbar\omega_p/E_{\rm J} = 7.9$ and zero magnetic flux. The degeneracy is seen to be fairly robust with respect to $E_{\rm J}$ disorder. The vertical line at 20% disorder marks the worst-case disorder seen in experiments. (b) Density plots of the ground-state wave function showing the expected deformation as $E_{\rm J}$ disorder is increased.

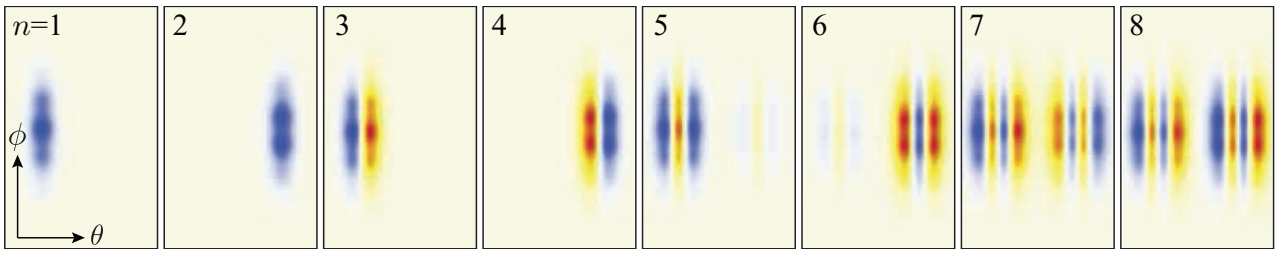

FIG. 8. (Color online) Density plot of low-lying wave functions with disjoint support. The numbers $n = 1,2,\ldots$ enumerate the eigenstates starting from the ground state. [Same parameters as in Fig. 4(b).]

the example parameters discussed in Sec. III, this frequency is approximately 280 MHz.) Due to disjoint support of wave functions as well as parity, we expect certain instances of the occurring matrix elements to be strongly suppressed; see Figs. 8 and 9(b).

Following the general approach from Ref. [35], we obtain the dispersive Hamiltonian

$$H' = \sum_{l=0}^{\infty} \left(E_l^{\rm sym} + \kappa_l\right)|l\rangle\langle l| + \hbar\Omega_\chi a^\dagger a + \sum_l \chi_l |l\rangle\langle l| a^\dagger a, \tag{19}$$

where

$$\chi_l = \sum_{l'} |g_{ll'}|^2 \left(\frac{1}{\Delta_{ll'}} - \frac{1}{\Delta_{l'l}}\right), \quad \kappa_l = \sum_{l'} \frac{|g_{ll'}|^2}{\Delta_{ll'}} \tag{20}$$

are the ac Stark shift and the Lamb shift, respectively. The detuning is defined as $\Delta_{ll'} = E_l^{\rm sym} - E_{l'}^{\rm sym} - \hbar\Omega_\chi$. We note that if there are resonances between the 0-π circuit and the harmonic oscillator, this perturbative treatment may break down. For small disorder, we expect that the Lamb shifts κ_l will be small compared to the splitting between each doublet.

V. CONCLUDING REMARKS

We have developed a full circuit analysis of the 0-π superconducting circuit, which is valid both in the highly degenerate regime as well as in intermediate parameter regimes where both the ground state and low-lying excited states are important. We find that in the case of symmetric parameter values and no disorder, the system can be decomposed into an uncoupled harmonic degree of freedom, and a subsystem subject to a two-dimensional effective potential. In a certain regime, the spectrum of this subsystem consists of degenerate doublets whose ground-state splitting is exponentially small compared with the spacing between the lowest two doublets ($\approx\omega_p\sqrt{E_{C\Sigma}/E_{CJ}}$). If such degenerate states could be utilized as quantum bits, they would be protected from both dephasing and relaxation and would not require fine-tuning of parameters. However, realizing universal operations on such states is not a trivial task, and is still a subject of active inquiry. Reaching the degenerate regime of $D > 2$ (a 100-fold suppression) requires realizing inductances slightly larger than the current state-of-the-art but seems possible with continued advances in design and microfabrication techniques.

A careful study of the effects of disorder has been presented. Deep within the degenerate regime, even large disorder in the circuit parameters will not strongly affect the degeneracy. In intermediate regimes, it is clear that disorder becomes important, especially disorder which introduces coupling to the χ harmonic mode. We have shown that this coupling can be treated using the formalism of circuit QED. Future work will consider the potential to exploit this additional quantum degree of freedom for quantum manipulation and readout.

In this context, understanding the effects of thermal fluctuations and relevant decoherence channels will also become important. Qualitatively, we expect exponential suppression of sensitivity to both charge and flux noise for $D > 1$. The charge noise sensitivity is similar to the suppression established in the transmon qubit [33,36] and is governed by the large ratio of $E_J/E_{C\Sigma}$. The reduced sensitivity to flux noise follows the same principle as for metaplasmon states in the fluxonium qubit [25,31]. The exponential insensitivity to offset charges also indicates robustness with respect to quasiparticle tunneling. However, this expectation should be verified in a future study using the general theory presented in Refs. [37–39].

The 0-π circuit and the analysis method we have employed point to a new strategy of engineering the potential and kinetic energies of circuits with larger numbers of degrees of freedom: the realization of protected manifolds, suitable for quantum information processing, through the design of potential landscapes with specific properties. Even in the absence of strict degeneracy, the presence of doublet λ systems in the energy spectrum represents a promising route to realizing ultracoherent qubits. Finally, it may be possible to employ more complex circuit topologies in the future design of potential-energy landscapes.

ACKNOWLEDGMENTS

We thank A. Houck, J. Lawrence, A. C. Y. Li, D. McKay, T. Yu, and G. Zhu for stimulating discussions. This research was supported by the NSF under Grants No. PHY-1055993 (J.D., B.F., D.G.F., J.K.), No. DMR-0805277 (D.G.F.), No. DMR-1151839 (D.I.S.), by the US Army Research Office under Grant No. W911NF-12-1-0608 (D.I.S.), by the Sloan Foundation (D.I.S.), and by the Packard Foundation (D.I.S.).

APPENDIX A: NUMERICAL DIAGONALIZATION OF THE 0-π HAMILTONIAN

For numerical diagonalization of the 0-π circuit Hamiltonian, we employ the finite-difference method in its simplest possible form. We truncate ϕ to a finite interval $[-\phi_M,\phi_M]$ and discretize ϕ and θ according to $\phi_m = m\Delta_\phi$

$(m = 0, \pm 1, \ldots, \pm M)$ and $\theta_n = n\Delta_\theta$ $(n = 1, \ldots, N)$ so that $\theta_N = N\Delta_\theta = 2\pi$. The corresponding orthonormal set $\{|nm\rangle\}$ of discretized position states is defined in the usual way by $\psi_{nm}(\phi,\theta) = \langle\phi,\theta \mid nm\rangle = (\Delta_\phi\Delta_\theta)^{-1/2}$ whenever (ϕ,θ) lies inside the rectangle centered at (ϕ_n,θ_m) with width and length set by the grid constants Δ_ϕ, Δ_θ. Everywhere else, the wave function vanishes. For sufficiently fine grid, the matrix elements of potential energy and kinetic energy are approximated by using $\langle m'n'|V(\phi,\theta)|mn\rangle \approx \delta_{mm'}\delta_{nn'}V(\phi_m,\theta_n)$ and

$$\langle m'n'|\partial_\phi^2|mn\rangle \approx \Delta_\phi^{-2}(\delta_{m',m+1}\delta_{n'n} + \delta_{m',m-1}\delta_{n'n} - 2\delta_{m'm}\delta_{n'n}),$$
$$\langle m'n'|\partial_\theta^2|mn\rangle \approx \Delta_\theta^{-2}(\delta_{m'm}\delta_{n',n+1} + \delta_{m'm}\delta_{n',n-1} - 2\delta_{m'm}\delta_{n'n}).$$

With this, the stationary Schrödinger equation reduces to a sparse eigenvalue problem which we solve numerically, while carefully checking for discretization errors and convergence.

APPENDIX B: CHARGE BASIS DISCUSSION OF WAVE FUNCTIONS AND DEGENERACY

To complement the flux space analysis given in the main text, in this appendix we discuss the energy levels and wave functions of the 0-π circuit from the perspective of the conjugate charge variables. Starting with the simple separable model of Eq. (9), then using a Bloch wave formalism [31], we describe how the ground-state doublet of the symmetric 0-π circuit is composed of states with even and odd charge parity.

To perform the switch to charge basis, we define a conjugate charge momentum $n_i^\vartheta = (n_\theta,n_\phi,n_\chi,n_\Sigma)_i$ for each flux variable $\vartheta_i = (\theta,\phi,\chi,\Sigma)_i$. The spectra of these charge operators can be discrete or continuous. For example, since n_θ is conjugate to the 2π-periodic variable θ, its eigenvalues are integer-valued and hence quantized. In contrast, the spectrum of n_ϕ is continuous and encompasses all $\mathbb{R}$. The spectrum of each charge operator determines the effects of offset charges coupling to it. In particular, since static offset charges do not affect continuous charge variables, we only need to consider the effects of a single offset charge n_g coupling to n_θ.

We can thus fully account for the effects of static offset charge in the 0-π circuit via the replacement $n_\theta \to (n_\theta - n_g)$. We use the notation $H_{\mathrm{sym}+n_g}$ to indicate the symmetric Hamiltonian of Eq. (8) under this replacement. As the relevant charging energy $E_{C\Sigma}$ is much smaller than the Josephson energy E_J, the eigenenergies of the 0-π circuit are exponentially insensitive to offset charge. We shall show how this insensitivity to offset charge is helpful in understanding the near degeneracy of the ground-state doublet.

The wave functions in charge basis ("momentum") now simply correspond to the Fourier components of the generalized flux basis ("position"), i.e.,

$$\tilde{\psi}(n_\theta,n_\phi) = \int_0^{2\pi}\frac{d\theta}{2\pi}\int_{-\infty}^{\infty}d\phi\, e^{-i(n_\theta\theta+n_\phi\phi)}\psi(\theta,\phi), \quad \text{(B1)}$$

or, in discretized form appropriate for the numerical implementation based on Appendix A,

$$\tilde{\Psi}_{\mu\nu} = \frac{1}{\sqrt{N(2M+1)}}\sum_{n,m} e^{-i[\nu n/N+\mu m/(2M+1)]}\Psi_{nm}. \quad \text{(B2)}$$

Figure 9 displays the charge basis form of the same wave functions presented in Fig. 4 (there shown in the generalized flux basis).

1. Charge parity and the ground-state doublet of a symmetric double well

To explain how insensitivity of the eigenenergies to offset charge and a conserved charge parity can lead to a nearly degenerate ground-state doublet, we first consider the simpler setting of the separable model discussed in the main text [see paragraph containing Eq. (9)]. For clarity, in this appendix we neglect the harmonic ϕ variable, considering only a one-dimensional Hamiltonian $H_{\mathrm{dw}+n_g}$ that includes the double-well potential $V_{\mathrm{dw}}(\theta) = |\cos(\theta)|$ and offset charge dependence. As V_{dw} is π periodic with only even Fourier components, if it were to describe a Josephson junction it would be a very special type of junction, allowing only even numbers of Cooper pairs to hop

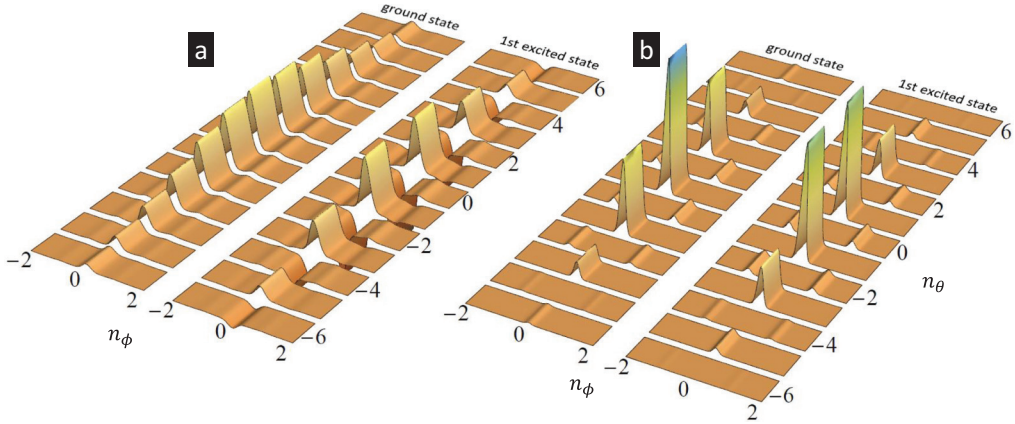

FIG. 9. (Color online) Charge-basis eigenfunctions for the nearly degenerate ground-state doublet of the symmetric 0-π circuit as described in Appendix B. Panels (a) and (b) respectively show the same states shown in Figs. 4(a) and 4(b) (there presented in the flux basis). In (b) the small splitting of the doublet is primarily determined by differences in the charging energy of the states. Each wave function has nearly disjoint support in the charge basis, and are located on interpenetrating "even" and "odd" quasicharge lattices (checkerboard pattern). In (a), the wave functions consist of symmetric and antisymmetric combinations of even and odd quasicharge wave functions. In this case, the energy splitting is primarily determined by the inductive energy which mixes states with different quasicharge parity.

together across it. To explain how such "even only" hopping leads to even and odd charge parity eigenstates, we introduce a charge parity operator

$$P = e^{\pi\partial_\theta} = e^{i\pi n_\theta}. \tag{B3}$$

The parity operator P commutes with $H_{\mathrm{dw}+n_g}$ and has two eigenspaces, an even subspace with eigenvalue $+1$ spanned by even charge states $|n_\theta \in \text{even}\rangle$, and an odd subspace with eigenvalue -1 spanned by $|n_\theta \in \text{odd}\rangle$. The Hamiltonian $H_{\mathrm{dw}+n_g}$ can be block-diagonalized in each parity subspace, with eigenvectors assigned either even or odd parity.

We now show how exponentially weak offset charge energy dispersion can help explain the existence of a ground-state doublet. To begin we note that the spectrum of $H_{\mathrm{dw}+n_g}$ has unit periodicity with respect to the offset charge n_g. To see this, consider that a change in offset charge $n_g \to n_g + 1$ can be exactly compensated by changing the eigenvectors $|\psi\rangle \to e^{i\theta}|\psi\rangle$, i.e., by $\sum_n \psi_n|n\rangle \to \sum_n \psi_n|n+1\rangle$ so that the eigenenergy remains invariant. While the spectrum of the Hamiltonian is invariant under such a shift in offset charge, the transformation $e^{i\theta}$ acts nontrivially on eigenstates, changing parity even states into parity odd states.

As known from the transmon limit of the Cooper pair box [33], the charge dispersion of the low-energy wave functions is exponentially suppressed when the charging energy is weak relative to the Josephson energy. Thus, while low-energy eigenstates of $H_{\mathrm{dw}+n_g}$ change their energy very little as a function of offset charge, the energy of an even eigenstate for offset charge n_g must be equal to the energy of an odd eigenstate for offset charge $n_g + 1$. As a result the low-energy eigenstates of $H_{\mathrm{dw}+n_g}$ in the $E_{\mathrm{CJ}} \ll E_{\mathrm{J}}$ limit will necessarily come in pairs. In particular, the ground state of $H_{\mathrm{dw}+n_g}$ will form a nearly degenerate doublet. The parity of the exact ground state depends on the particular value of n_g, with the even and odd eigenstates becoming exactly degenerate at $n_g = 1/2$.

In the main text, we emphasized the intuitive picture that decreasing tunneling through the double-well barrier leads to *localization* of wave functions in θ and near degeneracy. In the charge basis, the same intuition implies that increased *delocalization* of wave functions in n_θ generates the near degeneracy of the even and odd charge parity eigenstates.

2. Bloch wave analysis and the quasicharge double well

Just as for the simple one-dimensional (1D) model of the previous subsection, arguments based on charge parity and exponentially weak offset charge energy dispersion are helpful in explaining the ground-state doublet of the symmetric 0-π circuit, particularly from the perspective of the charge basis. However, for the symmetric 0-π circuit, the Hamiltonian is 2π periodic in θ (rather than π periodic like $H_{\mathrm{dw}+n_g}$). Also, the variable θ is strongly coupled to the continuous variable ϕ. Thus, the notion of charge parity is not as straightforward.

In this subsection we introduce a Bloch wave formalism [31] which allows us to define a notion of charge parity similar to the previous 1D example. To begin, we group together the noninductive terms of the symmetric 0-π Hamiltonian (including offset charge) defining

$$H_{\mathrm{sym}+n_g} = \tilde{H} + \tfrac{1}{2}E_L\phi^2, \tag{B4}$$

$$\tilde{H} = -2E_{\mathrm{C}\Sigma}(\partial_\theta - in_g)^2 + 2E_{\mathrm{CJ}}\partial_\phi^2 - 2E_{\mathrm{J}}\cos(\theta)\cos(\phi). \tag{B5}$$

The collected terms, $\tilde{H}$, are periodic in the continuous variable ϕ and are invariant under the primitive translation

$$T = e^{\pi\partial_\phi}e^{\pi\partial_\theta} = e^{i\pi n_\theta}e^{i\pi n_\phi}. \tag{B6}$$

We next define a Bloch wave basis as the simultaneous eigenvectors of $\tilde{H}$ and T,

$$T|q,s\rangle = e^{i\pi q}|q,s\rangle, \tag{B7}$$

$$\tilde{H}|q,s\rangle = \tilde{E}_s(q)|q,s\rangle, \tag{B8}$$

where $q \in [0,2)$ is a continuous quasicharge index and $s \in \{0,1,2,\ldots\}$ is a discrete quantum number.

Eigenstates within the quasicharge q subspace are spanned by charge states $|n_\theta,n_\phi\rangle$ that satisfy the relation

$$n_\phi + n_\theta \equiv q \pmod 2. \tag{B9}$$

These spanning states can be visualized as forming a checkerboard pattern in n_θ,n_ϕ charge space, where the checkerboard is offset from the origin in the n_ϕ direction by a distance q.

The significance of relation (B9) can be elucidated as follows. Consider the operators $e^{i(\theta+\phi)}$ and $e^{i(\theta-\phi)}$. The operator $e^{i(\theta+\phi)}$ describes a Cooper pair hopping across the Josephson junction with energy E_{J1}, while $e^{i(\theta-\phi)}$ describes a Cooper pair hopping across the Josephson junction with energy E_{J2} (see Fig. 1). As is clear from their definition, both operators individually change n_θ and n_ϕ by ± 1. Thus, the sum of the two remains within the same quasicharge subspace as expressed by Eq. (B9). In short, the Josephson hopping of Cooper pairs across either junction does not change the value of the quasicharge.

The $q = 0$ subspace includes charge states of the form $|n_\theta \in \text{even},n_\phi = 0\rangle$, while the $q = 1$ subspace includes charge eigenstates of the form $|n_\theta \in \text{odd},n_\phi = 0\rangle$. This similarity to the even and odd parity eigenstates of $H_{\mathrm{dw}+n_g}$ motivates our extension of the term even to indicate quasicharge states with a q value (mod 2) near zero, and odd to indicate quasicharge states with a q value (mod 2) near unity.

As discussed in the main text, degeneracy can arise when tunneling in the ϕ direction is much stronger than tunneling in the θ direction ($E_{\mathrm{C}\Sigma} \ll E_{\mathrm{CJ}}$). In addition, localization must occur in the θ direction ($E_{\mathrm{C}\Sigma} \ll E_{\mathrm{J}}$). In the charge basis this implies that wave functions should be delocalized in n_θ and, at the same time, considerably more localized in n_ϕ.

We next discuss the implications of these limits for the dependence of the band energies $\tilde{E}_s(q)$ on quasicharge q, and contrast it with the dispersion of $\tilde{E}_s(q)$ with respect to offset charge n_g. Just as for $H_{\mathrm{dw}+n_g}$, the spectrum of $\tilde{H}$ is offset charge periodic with period 1. The same argument applies: as offset charge changes by 1, $n_g \to n_g + 1$, the eigenvectors transform $|\psi\rangle \to e^{i\theta}|\psi\rangle$ so that the energy remains invariant. Importantly, under this transformation the value of the quasicharge changes $q \to q + 1$, interchanging even and odd parity states. This observation implies that in the

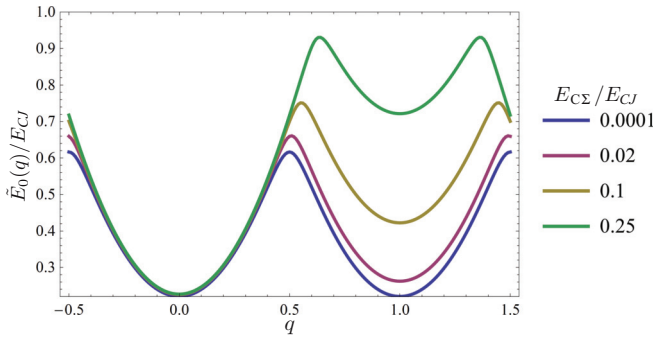

FIG. 10. (Color online) In the limit that the inductive energy goes to zero, the eigenfunctions of the symmetric 0-π Hamiltonian can be diagonalized within a Bloch wave formalism and assigned a quasicharge q. The figure shows the dependence of the energy of the lowest energy band $\tilde{E}_{s=0}(q)$ as a function of q. As the charging energy $E_{C\Sigma}$ decreases, states with quasicharges differing by 1 become nearly degenerate, leading to an effective quasicharge double well. Restoring the inductive energy but maintaining the limit of large inductance leads to a doublet comprised of a state with even quasicharge [$q \pmod 2 \approx 0$] and odd quasicharge [$q \pmod 2 \approx 1$].

limit of small $E_{C\Sigma}$ but $E_J \approx E_{CJ}$, states with quasicharge q and $q+1$ will become nearly degenerate, i.e., $\tilde{E}_s(q) \approx \tilde{E}_s(q+1)$, yet despite this, $E_s(q)$ retains strong dispersion with q.

Figure 10 shows a numerical calculation of the dependence of the energy of the lowest band on quasicharge, $\tilde{E}_0(q)$, for different values of $E_{C\Sigma}$. The calculation shows the onset of unit periodicity of $\tilde{E}_0(q)$ in the limit of small $E_{C\Sigma}$. Even in this limit, the dispersion of $\tilde{E}_0(q)$ with q remains of order E_{CJ}. We will refer to this as a quasicharge double well.

3. Ground-state doublet of the symmetric 0-π Hamiltonian

We now use the Bloch wave basis introduced in the previous subsection to analyze the symmetric 0-π Hamiltonian. As expressed in Eq. (B4) the Hamiltonian $H_{\mathrm{sym}+n_g}$ is comprised of terms, $\tilde{H}$, which are diagonal in the Bloch wave basis, as well as the term, $E_L\phi^2/2$, which accounts for the inductive energy. As the inductive term is not periodic under the translation T the Hamiltonian $H_{\mathrm{sym}+n_g}$ will not conserve quasicharge. However, the operator ϕ *does* act locally in the quasicharge basis with a contribution proportional to ∂_q. Explicitly we have

$$\langle q,s|\phi|q',s'\rangle = \delta(q-q')[i\delta_{ss'}\partial_q - \Omega(q)_{ss'}]. \tag{B10}$$

Here, the gauge potential Ω is defined as

$$\langle \phi|q,s\rangle = e^{iq\phi}u_s(q,\phi), \tag{B11}$$

$$\Omega(q)_{ss'} = \frac{i}{2\pi}\oint d\phi\, u_s^*(q,\phi)\partial_q u_{s'}(q,\phi). \tag{B12}$$

Since Ω also becomes unit periodic in q in the limit of small $E_{C\Sigma}$, for a qualitative understanding it is sufficient to neglect its effects and approximate $E_L\phi^2 \approx -E_L\partial_q^2$. In the limit that $E_L \ll E_{CJ}$ the large values of inductance allow the low-energy wave functions to reduce their tunneling in the q direction and localize within each even and odd well, forming a ground-state doublet.

To help understand the remarkable properties of such large inductance scales it is useful to consider the case of a superconducting L-C oscillator. For conventional superconducting L-C oscillators the impedance $\sqrt{L/C}$ is small compared to the superconducting impedance quantum $\hbar/(2e)^2 \approx 1.02\ \mathrm{k}\Omega$. This implies that the low-energy eigenfunctions have charge fluctuations that are significantly larger than that of a single Cooper pair. One remarkable property of a superinductor is that it allows for impedance values to be in the opposite regime, generating low-energy eigenfunctions with charge number fluctuations comparable to or smaller than that of a single Cooper pair.

4. Splitting of the ground-state doublet

Now that we have discussed the formation of the ground-state doublet of the symmetric 0-π circuit from the charge perspective, we parallel the main text and discuss the small remaining splitting and the structure of the eigenfunctions. As discussed in the main text, in the limit of $E_{C\Sigma}$ large and E_L small, the doublet is primarily split by tunneling in the θ direction [case (b) of Fig. 4]. In the charge basis this limit corresponds to large enough $E_{C\Sigma}$ so that the remaining energy difference on either side of the quasicharge double well primarily determines the splitting of the doublet [case (b) of Fig. 9]. In the opposite limit [E_L large and $E_{C\Sigma}$ small; cases (a) of Figs. 4 and 9] the flux space intuition is that the doublet is split by the energy differences on the two sides of the flux space potential ridges. The charge space interpretation is that the doublet is split primarily due to inductance-induced tunneling through the barrier of the quasicharge double well.

We can now use this analysis to understand the charge space structure of the ground-state doublet eigenfunctions (for $n_g = 0$ and $\varphi_{\mathrm{ext}} = 0$). When the eigenfunctions are located within separate parity wells [$E_{C\Sigma}$ large and E_L small; Fig. 9(b)], the peaks in amplitude of the charge space eigenfunctions take the form of a checkerboard with a small spread of order Δq in n_ϕ around each peak—with the magnitude of the peaks decreasing more slowly in the n_θ direction. (Here, Δq is the oscillator length in the local minimum of the quasicharge double well.) The two eigenfunctions of the doublet are spaced on interpenetrating sublattices. In the opposite limit [E_L large and $E_{C\Sigma}$ small; Fig. 9(a)], the eigenfunctions become the symmetric and antisymmetric superposition of such checkerboard wave functions.

We conclude this appendix by emphasizing one important way in which the near-degeneracy of the superconducting 0-π circuit differs from the degeneracy of a conventional double well that can occur in, e.g., a flux qubit. For a conventional double well any stray magnetic field that couples to ϕ will bias the minimums on either side of the potential barrier, and will lift the degeneracy. Fluctuations of such magnetic fields will lead to dephasing. For the 0-π circuit an analogous operator that lifts the degeneracy is any operator that mixes states with even and odd parity such as $e^{i\theta}$. However, such operators involve coherent hopping of Cooper pairs across insulating barriers, and thus can be dramatically suppressed. Nevertheless, such considerations may lead to some practical design limits, e.g., on the minimum thickness of the insulating barrier between the large capacitors of the 0-π circuit.

[1] A. Y. Kitaev, Ann. Phys. **303**, 2 (2003).
[2] C. Nayak, A. Stern, M. Freedman, and S. Das Sarma, Rev. Mod. Phys. **80**, 1083 (2008).
[3] D. A. Abanin, Z. Papić, Y. Barlas, and R. N. Bhatt, New J. Phys. **14**, 025009 (2012).
[4] N. Read and D. Green, Phys. Rev. B **61**, 10267 (2000).
[5] F. Hassler, A. R. Akhmerov, C.-Y. Hou, and C. W. J. Beenakker, New J. Phys. **12**, 125002 (2010).
[6] J. Alicea, Y. Oreg, G. Refael, F. von Oppen, and M. P. A. Fisher, Nat. Phys. **7**, 412 (2011).
[7] L. Jiang, C. L. Kane, and J. Preskill, Phys. Rev. Lett. **106**, 130504 (2011).
[8] F. Hassler, A. R. Akhmerov, and C. W. J. Beenakker, New J. Phys. **13**, 095004 (2011).
[9] B. van Heck, A. R. Akhmerov, F. Hassler, M. Burrello, and C. W. J. Beenakker, New J. Phys. **14**, 035019 (2012).
[10] D. Pekker, C.-Y. Hou, V. E. Manucharyan, and E. Demler, Phys. Rev. Lett. **111**, 107007 (2013).
[11] H. Paik, D. I. Schuster, L. S. Bishop, G. Kirchmair, G. Catelani, A. P. Sears, B. R. Johnson, M. J. Reagor, L. Frunzio, L. I. Glazman, S. M. Girvin, M. H. Devoret, and R. J. Schoelkopf, Phys. Rev. Lett. **107**, 240501 (2011).
[12] C. Rigetti, J. M. Gambetta, S. Poletto, B. L. T. Plourde, J. M. Chow, A. D. Córcoles, J. A. Smolin, S. T. Merkel, J. R. Rozen, G. A. Keefe, M. B. Rothwell, M. B. Ketchen, and M. Steffen, Phys. Rev. B **86**, 100506 (2012).
[13] Y. Nakamura, Y. Pashkin, and J. Tsai, Nature (London) **398**, 786 (1999).
[14] V. Bouchiat, D. Vion, P. Joyez, D. Esteve, and M. H. Devoret, Phys. Scr. **T76**, 165 (1998).
[15] M. H. Devoret and J. M. Martinis, Quantum Inf. Process. **3**, 163 (2004).
[16] J. Clarke and F. Wilhelm, Nature (London) **453**, 1031 (2008).
[17] R. J. Schoelkopf and S. M. Girvin, Nature (London) **451**, 664 (2008).
[18] M. H. Devoret and R. J. Schoelkopf, Science **339**, 1169 (2013).
[19] B. Douçot and J. Vidal, Phys. Rev. Lett. **88**, 227005 (2002).
[20] B. Douçot, L. B. Ioffe, and J. Vidal, Phys. Rev. B **69**, 214501 (2004).
[21] S. Gladchenko, D. Olaya, E. Dupont-Ferrier, B. Douçot, L. B. Ioffe, and M. E. Gershenson, Nat. Phys. **5**, 48 (2008).
[22] B. Douçot and L. B. Ioffe, in *Advances in Theoretical Physics: Landau Memorial Conference*, edited by V. Lebedev and M. Feigel'man, AIP Conf. Proc. No. 1134 (AIP, Melville, NY, 2009), p. 128.
[23] B. Douçot and L. B. Ioffe, Rep. Prog. Phys. **75**, 072001 (2012).
[24] P. Brooks, A. Kitaev, and J. Preskill, Phys. Rev. A **87**, 052306 (2013).
[25] V. E. Manucharyan, J. Koch, L. I. Glazman, and M. H. Devoret, Science **326**, 113 (2009).
[26] V. E. Manucharyan, N. A. Masluk, A. Kamal, J. Koch, L. I. Glazman, and M. H. Devoret, Phys. Rev. B **85**, 024521 (2012).
[27] M. T. Bell, I. A. Sadovskyy, L. B. Ioffe, A. Y. Kitaev, and M. E. Gershenson, Phys. Rev. Lett. **109**, 137003 (2012).
[28] N. A. Masluk, I. M. Pop, A. Kamal, Z. K. Minev, and M. H. Devoret, Phys. Rev. Lett. **109**, 137002 (2012).
[29] M. H. Devoret, in *Quantum Fluctuations*, Proceedings of the Les Houches Summer School, Session LXIII (Elsevier, Amsterdam, 1997), Chap. 10.
[30] G. Burkard, R. H. Koch, and D. P. DiVincenzo, Phys. Rev. B **69**, 064503 (2004).
[31] J. Koch, V. E. Manucharyan, M. H. Devoret, and L. I. Glazman, Phys. Rev. Lett. **103**, 217004 (2009).
[32] D. G. Ferguson, A. A. Houck, and J. Koch, Phys. Rev. X **3**, 011003 (2013).
[33] J. Koch, T. M. Yu, J. M. Gambetta, A. A. Houck, D. I. Schuster, J. Majer, A. Blais, M. H. Devoret, S. M. Girvin, and R. J. Schoelkopf, Phys. Rev. A **76**, 042319 (2007).
[34] A. Blais, R.-S. Huang, A. Wallraff, S. M. Girvin, and R. J. Schoelkopf, Phys. Rev. A **69**, 062320 (2004).
[35] G. Zhu, D. G. Ferguson, V. E. Manucharyan, and J. Koch, Phys. Rev. B **87**, 024510 (2013).
[36] J. A. Schreier, A. A. Houck, J. Koch, D. I. Schuster, B. R. Johnson, J. M. Chow, J. M. Gambetta, J. Majer, L. Frunzio, M. H. Devoret, S. M. Girvin, and R. J. Schoelkopf, Phys. Rev. B **77**, 180502(R) (2008).
[37] G. Catelani, J. Koch, L. Frunzio, R. J. Schoelkopf, M. H. Devoret, and L. I. Glazman, Phys. Rev. Lett. **106**, 077002 (2011).
[38] G. Catelani, R. J. Schoelkopf, M. H. Devoret, and L. I. Glazman, Phys. Rev. B **84**, 064517 (2011).
[39] G. Catelani, S. E. Nigg, S. M. Girvin, R. J. Schoelkopf, and L. I. Glazman, Phys. Rev. B **86**, 184514 (2012).